TABLE 3 Deviations from Hardy–Weinberg genotype proportions at 10 polymorphic loci in polygyne *S. invicta*

	Aat-2	*Acoh-1*	*Acoh-5*	*Acy1*	*Ddh-1*	*Est-4*	*Est-6*	*G3pdh-1*	*Pgm-1*	*Pro-5*
Workers										
larvae ($N=31$, $n=1012$)	0	—	—	—	0.02	0	—	—	0	—
pupae ($N=31$, $n=1015$)	—	0	0	—	—	—	0	—	0.04	—
adults ($N=31$, $n=976$)	0	—	—	—	—	0.04	—	0	0	—
Queens										
wingless reproductives ($N=31$, $n=616$)	0	0	0	—	—	0.02	—	0	0.02	—
winged nonreproductives ($N=31$, $n=954$)	0.02	0	—	0	—	0.04	—	0.02	0.04	0.02

N, Number of nests; *n*, mean number of individuals studied per locus for each class of female. Values represent the proportion of 50 random draws of single genotypes per nest in which the ratios of the drawn genotypes departed significantly from those expected under Hardy–Weinberg equilibrium (χ^2 test with Yates' continuity correction, 5% significance level; see Table 1 legend). Dashes indicate that the markers were not scored in a particular material. Genotypes were scored following horizontal electrophoresis in 14% starch gels using a pH 6.0 amine-citrate (morpholine) continuous buffer system (*Ddh-1, Est-4, Est-6, G3pdh-1, Pgm-1, Pro-5*), a pH 8.6 Tris-borate-EDTA continuous buffer system (*Aat-2, Acy1*), or a pH 6.5 Tris-citrate continuous buffer system (*Acoh-1, Acoh-5*), with the protein bands visualized by specific histochemical staining[12,28,29]. Mendelian inheritance of all 10 markers has been confirmed by family studies (ref. 12; D. Shoemaker, J. Costa and K.G.R., manuscript in preparation).

queens homozygous for *Pgm-3*^{a} suggests that the dynamics of this allele should mimic those of a recessive lethal, resulting in virtual monomorphism for the alternate allele in relatively few generations in the absence of other evolutionary forces[20]. Yet *Pgm-3*^{a} was common in the polygyne population over both years of this study. Because a high frequency of this allele in polygyne males can be ruled out as an explanation for the maintenance of this polymorphism (Table 1), the most likely cause is that *Pgm-3*^{a} is continually reintroduced into the polygyne population through dispersing monogyne males. *Pgm-3*^{a} occurs at high frequency in these males (Table 1), and their ability to disperse widely[21] and the modest size of the polygyne population studied[22] allow ample opportunity for males from surrounding monogyne populations to reach polygyne females. Moreover, the *Pgm-3*^{a} allele is sufficiently more common in monogyne males than in polygyne reproductive queens that substantial excess heterozygosity should be generated at *Pgm-3* if they interbreed[20], as is observed. Indeed, the excess heterozygosity found in nonreproductive polygyne females can be fully accounted for if some 80% of matings in the polygyne population involve monogyne males (Fig. 1). Additionally, the distribution of genotype classes observed in 69 families derived from single polygyne queens closely matches the distribution expected if monogyne males are responsible for 80% of the matings (Table 2). Finally, because of reduced allelic variation at the putative sex-determining locus, 80–95% of males produced in polygyne populations of *S. invicta* are infertile diploids, whereas males in monogyne populations are invariably haploid[23–25]. Thus there may be too few fertile haploid males produced in polygyne populations to compete effectively with immigrant monogyne males for fertilizations.

This study provides evidence that a single gene can strongly influence the outcome of reproductive competition in a social insect, that this effect is dependent on social context, and that both selection and gene flow are important in determining genotype and allele frequencies at this gene in a specific social environment. Identification of the gene and physiological role of its product may elucidate the manner in which its phenotypic social effects are achieved and so provide a model for the genetic basis of queen competition and control in insect societies. □

Received 8 August; accepted 4 November 1991.

1. Wilson, E. O. *The Insect Societies* (Belknap, Cambridge, Massachusetts, 1971).
2. West-Eberhard, M. J. in *Natural Selection and Social Behavior: Recent Research and New Theory* (eds Alexander, R. D. & Tinkle, D. W.) 3–17 (Chiron, New York, 1981).
3. Fletcher, D. J. C. & Ross, K. G. *A. Rev. Entomol.* **30,** 319–343 (1985).
4. Strassmann, J. E. & Meyer, D. C. *Anim. Behav.* **31,** 431–438 (1983).
5. Sullivan, J. D. & Strassmann, J. E. *Behav. Ecol. Sociobiol.* **15,** 249–256 (1984).
6. Michener, C. D. in *Social Insects: An Evolutionary Approach to Castes and Reproduction* (ed. Engels, W.) 77–121 (Springer, Berlin, 1990).
7. Röseler, P.-F. in *The Social Biology of Wasps* (eds Ross, K. G. & Matthews, R. W.) 309–335 (Cornell University Press, Ithaca, 1991).
8. Fletcher, D. J. C. & Blum, M. S. *Science* **219,** 312–314 (1983).
9. Hölldobler, B. & Wilson, E. O. *The Ants* (Belknap, Cambridge, Massachusetts, 1990).
10. Velthuis, H. H. W., Ruttner, F. & Crewe, R. M. in *Social Insects: An Evolutionary Approach to Castes and Reproduction* (ed. Engels, W.) 231–243 (Springer, Berlin, 1990).
11. Moritz, R. F. A. & Hillesheim, E. *Behav. Ecol. Sociobiol.* **17,** 87–89 (1985).
12. Ross, K. G. & Fletcher, D. J. C. *Behav. Ecol. Sociobiol.* **17,** 349–356 (1985).
13. Vargo, E. L. & Fletcher, D. J. C. *Physiol. Entomol.* **12,** 109–116 (1987).
14. Markin, G. P., Collins, H. L. & Dillier, J. H. *Ann. ent. Soc. Am.* **65,** 1053–1058 (1972).
15. Glancey, B. M. & Lofgren, C. S. *Fla. Ent.* **71,** 581–587 (1988).
16. Vargo, E. L. & Porter, S. D. *Ann. ent. Soc. Am.* **82,** 307–313 (1989).
17. Fletcher, D. J. C. & Blum, M. S. *Science* **212,** 73–75 (1981).
18. Fletcher, D. J. C. in *Advances in Invertebrate Reproduction 4* (eds Porchet, M., Andries, J.-C. & Dhainaut, A.) 305–316 (Elsevier, Amsterdam, 1986).
19. Vargo, E. L. & Ross, K. G. *J. Insect Physiol.* **35,** 587–593 (1989).
20. Hedrick, P. W. *Genetics of Populations* (Jones & Bartlett, Boston, 1985).
21. Markin, G. P., Dillier, J. H., Hill, S. O., Blum, M. S. & Hermann, H. R. *J. Georgia ent. Soc.* **6,** 145–156 (1971).
22. Fletcher, D. J. C. *J. Georgia ent. Soc.* **18,** 538–543 (1983).
23. Hung, A. C. F., Vinson, S. B. & Summerlin, J. W. *Ann. ent. Soc. Am.* **67,** 909–912 (1974).
24. Ross, K. G. & Fletcher, D. J. C. *Evolution* **39,** 888–903 (1985).
25. Ross, K. G. & Fletcher, D. J. C. *Behav. Ecol. Sociobiol.* **19,** 283–291 (1986).
26. Crozier, R. H., Smith, B. H. & Crozier, Y. C. *Evolution* **41,** 902–910 (1987).
27. Weir, B. S. *Genetic Data Analysis* (Sinauer, Sunderland, Massachusetts, 1990).
28. Qavi, H. & Kit, S. *Biochem. Genet.* **18,** 669–679 (1980).
29. Murphy, R. W., Sites, J. W., Buth, D. G. & Haufler, C. H. in *Molecular Systematics* (eds Hillis, D. M. & Moritz, C.) 45–126 (Sinauer, Sunderland, Massachusetts, 1990).

ACKNOWLEDGEMENTS. I thank L. Keller, M. A. Moran, D. Shoemaker, J. Cook, M. Arnold, and J. Costa for advice and assistance. This work was supported in part by the National Geographic Society and the Georgia Agricultural Experiment Stations, University of Georgia.

Stationary and drifting spiral waves of excitation in isolated cardiac muscle

Jorge M. Davidenko, Arcady V. Pertsov, Remy Salomonsz, William Baxter & José Jalife

Department of Pharmacology, SUNY Health Science Center, 750 East Adams Street, Syracuse, New York 13210, USA

EXCITABLE media can support spiral waves rotating around an organizing centre[1–7]. Spiral waves have been discovered in different types of autocatalytic chemical reactions[8,9] and in biological systems[10–12]. The so-called 're-entrant excitation' of myocardial cells[13], causing the most dangerous cardiac arrhythmias, including ventricular tachycardia and fibrillation, could be the result of spiral waves[1,2]. Here we use a potentiometric dye[14,15] in combination with CCD (charge-coupled device) imaging technology[16,17] to demonstrate spiral waves in the heart muscle. The spirals were elongated and the rotation period, T_s, was about 180 ms (3–5 times faster than normal heart rate). In most episodes, the spiral was anchored to small arteries or bands of connective tissue, and gave rise to stationary rotations. In some cases, the core drifted away from its site of origin and dissipated at a tissue border. Drift was associated with a Doppler shift in the local excitation period, T, with T ahead of the core being about 20% shorter than T behind the core.

Sustained spiral-wave activity was consistently initiated in thin ($20 \times 20 \times 0.5$ mm) slices of sheep and dog epicardial muscle by crossfield stimulation[2,15,18]. The rotation period ($T_s = 183 \pm$

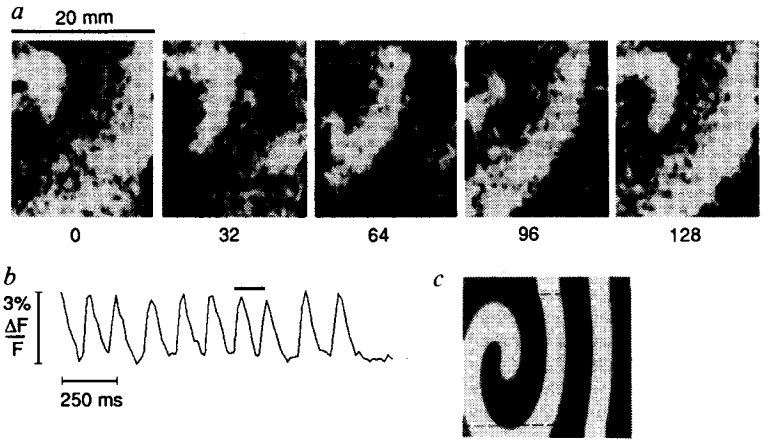

FIG. 1 *a*, Clockwise-rotating spiral wave in canine epicardial muscle. White, maximal depolarization; black, resting potential; numbers, time in ms. *b*, Time course of local activation on the upper left corner of the tissue during the last 10 cycles. Bar indicates time of recording in *a*. *c*, Snapshot of a spiral wave obtained in a computer simulation using the Fitz-Hugh-Nagumo model[23] in which anisotropy $D_x/D_y=4$ was introduced. Array size, 96×96. Dashed box roughly corresponds to the size of the heart preparation shown in *a*.

METHODS. Slices ($20\times20\times0.5$ mm) of epicardial muscle were obtained from sheep and dogs (10–20 kg) and superfused with oxygenated Tyrode solution[15] containing diacetyl monoxime (Sigma) 10–15 mM to abolish contractility[15,26]. Tissues were stained with 1.3 μg ml^{-1} di-4-ΔNEPPS (Molecular Probes, Eugene, Oregon). Stimuli were delivered through one of four pairs of Ag–AgCl electrodes, as described elsewhere[15]. Self-sustaining repetitive activity was initiated as a result of the intersection of two perpendicular planar waves[15]. Refractory period was measured by the S_1–S_2 protocol[19]. Fluorescence was excited at 490 nm and measured at 645 nm. Changes in fluorescence related to transmembrane potential changes[14–17], were recorded from an area of about 400 mm^2, with a spatial resolution up to 30 μm per pixel, at a rate of 60 frames s^{-1} and 8 bits. Digital subtraction of background fluorescence and spatial filtering were used. Equipment: Zenith 386 computer with a 361 Mbyte hard disk, an RGB colour monitor, a 4-Mybte video board (Epix) and a video camera (Cohu series 6500). Hard copies were obtained with a video copy processor (Mitsubishi P40U).

s.d. 68 ms; $n=33$) was 1.39 times longer than the refractory period ($T_r=131\pm38$ ms, $n=20$). A full revolution of a clockwise-rotating spiral and the pattern of local activation are shown in Fig. 1 *a*, *b*. The tip of the spiral has a pronounced curvature. As a result of the anisotropic properties of epicardial ventricular muscle[19], wave propagation in the long axis of the cells was 3.9 ± 2.2 times faster than in the transverse direction, which resulted in an elliptical spiral. A similar elliptical spiral is observed in generic reaction-diffusion equations when an equivalent anisotropy is introduced (Fig. 1*c*).

Spiral waves are considered stationary when the tip of the spiral, which circulates around the core, follows a closed circular or elliptical trajectory and the periodicity is preserved everywhere outside the core[20]. To characterize the size and location of the core we used a time-space plot ('frame stack') presentation. The time-space plots of the spiral wave (Fig. 2) have specific branching bands of lower amplitude in the centre of the plot which are divided in time by $T_s/2$. The distance between branching bands in the horizontal axis determines the effective size of the wave source (that is, the core) in this particular projection.

Figure 2*b* shows the frame-stack display of a recorded spiral wave. The rotating activity was stationary ($T_s=115$ ms) for more than 20 min (it was subsequently interrupted by applying external stimulation). The size of the core in the horizontal and vertical (not shown) projections was 1.1 mm and 9.7 mm, respectively. The size as well as the position of the core remained stable throughout the episode. The real image of the preparation showed that the core was anchored to the border of a small (1×12-mm) artery. In 14 episodes of stationary rotations analysed, the core was elongated (mean short and long axes, 3.1 ± 0.8 and 5.5 ± 1.5 mm, respectively), and in nine cases showed similar attachment to anatomical discontinuities.

To determine whether the low-voltage activity in the core was solely produced by such discontinuities or was functionally determined, the voltage structure of the preparation during spiral wave activity (Fig. 3*a*) was compared with that during planar wave propagation (Fig. 3*b*). Frame-stack plots were obtained sequentially from narrow rectangular sections across the core's centre (Fig. 3*a*, top). The amplitude of fluorescence (depolarization) of 50 superimposed frames taken from the same section is shown in Fig. 3*a*, bottom. The amplitude was lower in the core's centre than in the periphery. In addition, the minimum value was higher, thus indicating that the core region never reached full repolarization. Signals of normal amplitude were recorded in the same region of tissue during planar wave propagation (Fig. 3*b*). Indeed, although the region contained a small artery, activity was uniform throughout the segment, which demonstrated that the differences in fluorescence associated with spiral wave activity are determined by functional differences between the core and the periphery. In 14 episodes of stationary spiral waves, the core amplitude was $25\pm17\%$ of the absolute maximum amplitude. Similar characteristics have been described for the BZ reaction[21].

FIG. 2 *a*, Frame-stack display (similar to that in refs. 12, 27) of spiral wave activity obtained according to

$$\bar{F}(x,t)=\frac{1}{a}\int_0^a F(x,y,t)\,dy$$

$$\bar{F}(y,t)=\frac{1}{b}\int_0^b F(x,y,t)\,dx$$

$F(x,y,t)$ is fluorescence signal, $a\times b$ is frame size. In each frame ($t_1, t_2 \ldots t_n$), all pixel values of each column were added to form a single line, represented at the edge of the frame. Arrows indicate direction of propagation. Intensity of shading indicates level of F; tangent of α represents velocity of wave propagation. The $F(x,t)$ plot was obtained by stacking all 'frame-lines'. Black bands, excitation on either side of the core; T_s, vertical distance between two consecutive excitation bands; shaded bars, core. *b*, Frame-stack display (negative contrast) of a stationary spiral wave induced in sheep epicardial muscle ($a\times b=20\times26$ mm). White regions, excitation bands; black regions, at rest. $T_s=115$ ms.

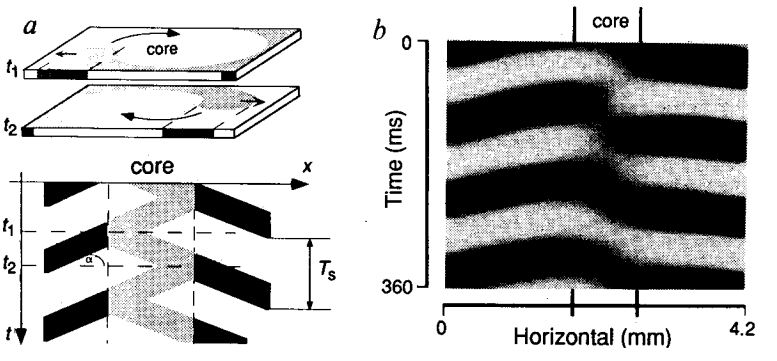

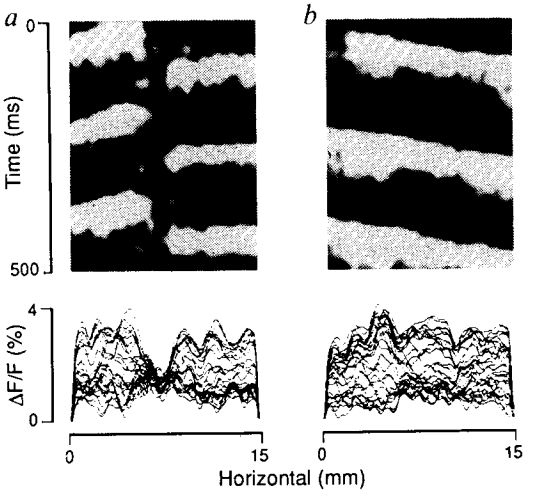

FIG. 3 *a*, Top: $F(x, t)$ plot of cross-section through centre of the core of a stationary spiral wave ($a \times b = 0.94 \times 15$ mm). Bottom: superimposed plots[22] of $\Delta F/F$; 50 frames (roughly six rotating cycles) in the same region as on top. *b*, $F(x, t)$ and $\Delta F/F$ plots obtained 10 min later from the same section as in *a* during planar wave propagation.

Nonstationary rotations occur when the core shifts its position giving rise to spatial and temporal irregularities in the activation[20–22]. Figure 4*a*, shows a frame-stack display obtained in one of seven episodes in which activity was nonstationary. The core initially appeared near the right border and slowly drifted 10 mm toward the left over a 1-s period (roughly seven cycles), in a direction that was perpendicular to the long axis of the cells, with no major changes in the vertical position (vertical frame-stack plot not shown). In general, however, the direction of the drift appeared to be independent of the cell orientation. In some cases the drift occurred in varying directions within the same preparation. Finally, in this experiment, the speed of wave front propagation in the direction of the drift was 90 mm s^{-1}. Overall, the average ratio of velocity of wave propagation over velocity of drift, was 9.8 ± 2.1 ($n = 7$).

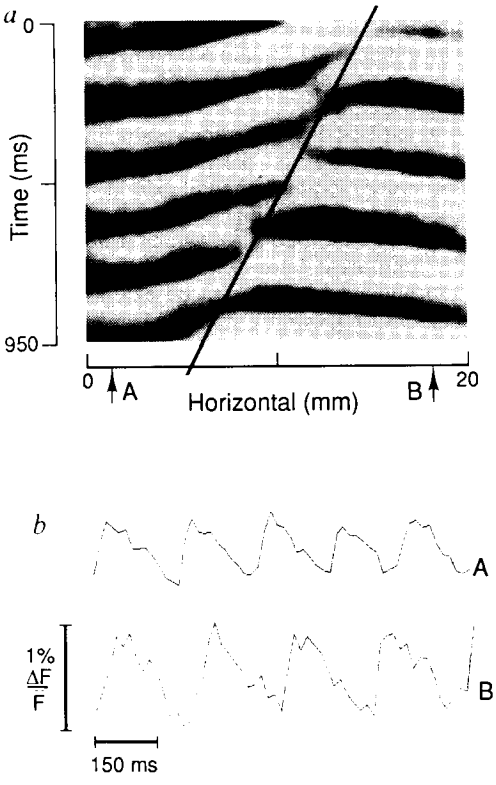

FIG. 4 *a*, $F(x, t)$ plot of a drifting spiral wave. Diagonal line follows the drift of the core in the horizontal axis. *b*, Pattern of local activation obtained from two points ahead and behind the core. The horizontal position of the selected points is indicated by the arrows in *a*. Mean T ahead (A) of the core was 175 ms; mean T behind (B) the core was 205 ms.

When the core of the drifting spiral collided with the border of the tissue, the spiral was annihilated and the rotations stopped. According to some theoretical suggestions[23], the spiral wave can interact with the boundary of the medium to result in drifting of the spiral along the boundary at a distance which is close to the critical radius, R_c (the minimum radius of that region which is necessary to maintain a spreading wave). In our experiments, however, the distance between the core and the border was never constant and there was no correlation between the border-to-core distance and drift velocity.

Drifting of the spiral wave resulted in a Doppler shift of the period of rotation (Fig. 4*b*). In the example shown, the rotation period ahead (A) of the core was 30 ms shorter than that behind (B), the core. In seven experiments, A (142 ± 27 ms) was always shorter than B (178 ± 35 ms). In some cases (Fig. 1), the drift direction varied, giving rise to aperiodic patterns of local activation (Fig. 1*b*). The analogy between spiral waves and re-entrant excitation which underlie life-threatening cardiac arrhythmias in experimental models[13,18,24] as well as in the human heart[25] is well known[1,2]. Our results strongly support this association. □

Received 8 October; accepted 14 November 1991.

1. Krinsky, V. I. (ed.) *Self-organization: Autowaves and Structures Far from Equilibrium* 9–18 (Springer, Berlin, 1984).
2. Winfree, A. T. *J. theor. Biol.* **138,** 353–405 (1989).
3. Keener, J. P. *J. appl. Math.* **46,** 1039–1056 (1986).
4. Gerhardt, M., Schuster, H. & Tyson, J. J. *Science* **247,** 1563–1566 (1990).
5. Markus, M. & Hess, B. *Nature* **347,** 56–58 (1990).
6. Wiener, N. & Rosenblueth, A. *Arch. Inst. Cardiol. Mex.* **16,** 205–265 (1946).
7. Krinsky, V. I. *Probl. Kibernetiki* **20,** 59–80 (1968).
8. Zhabotinsky, A. M. & Zaikin, A. N. *Oscillatory Processes in Biological and Chemical Systems* Vol. 2 279–283 (Pushchino, on Oka, 1971).
9. Winfree, A. T. *Science* **175,** 634–636 (1972).
10. Gerisch, G. *Curr. Topics dev. Biol.* **3,** 157– (1968).
11. Bures, J. & Gorelova, N. A. *J. Neurobiol.* **14,** 353–363 (1983).
12. Lechleiter, J., Girard, S., Peralta, E. & Clapham, D. *Science* **252,** 123–126 (1991).
13. Allessie, M. A., Bonke, F. I. M. & Shopman, F. J. G. *Circ. Res.* **33,** 54–62 (1973).
14. Salzberg, B. M., Davila, H. V. & Cohen, L. B. *Nature* **246,** 508–509 (1973).
15. Davidenko, J. M., Kent, P. F., Chialvo, D. R., Michaels, D. C. & Jalife, J. *Proc. natn. Acad. Sci. U.S.A.* **87,** 8785–8789 (1990).
16. Blasdel, G. G. & Salama, G. *Nature* **321,** 579–585 (1986).
17. Kauer, J. *Nature* **331,** 166–168 (1988).
18. Frazier, D. W. *et al. J. clin. Invest.* **83,** 1039–1052 (1989).
19. Delgado, C., Steinhaus, B., Delmar, M., Chialvo, D. R. & Jalife, J. *Circ. Res.* **67,** 97–110 (1990).
20. Zykov, V. S. in *Simulation of Wave Processes in Excitable Media* (ed. Winfree, A. T.) 93–112 (1987).
21. Muller, S. C., Plesser, T. & Hess, B. *Science* **230,** 661–663 (1985).
22. Fast, V. G. & Pertsov, A. M. *Biophysics* **35,** 478–481 (1990).
23. Ermakova, E. A. & Pertsov, A. M. *Biophysics* **31,** 855–861 (1986).
24. Cardinal, R., Savard, P., Carson, L., Jean-Benoit, P. & Page, P. *Circulation* **70,** 136–148 (1984).
25. Downar, E. *et al. J. Am. Coll. Card.* **4,** 703–714 (1984).
26. Li, T., Sperelakis, N., Teneick, R. E. & Solaro, J. R. *J. Pharmac. exp. Ther.* **232,** 688–695 (1985).
27. Yamaguchi, T. & Mueller, S. C. *Physica* D **49,** 40–46 (1991).

ACKNOWLEDGEMENTS. We thank J. Kauer and G. Cinelli for help in developing our video optical mapping system, L. Lowe for voltage-sensitive dyes, A. Winfree, R. Ideker, V. Krinsky and D. Michaels for reading the manuscript and W. Coombs and J. A. Getchonis for technical assistance. This work was supported by the NIH and the American Heart Association.